DETECTION OF GEODETIC DEFORMATION IN THE 2010 BAJA CALIFORNIA EARTHQUAKE FROM SATELLITE SAR IMAGES

Wen Liu[1], Masashi Matsuoka[2] and Fumio Yamazaki[3]

ABSTRACT

A M_W 7.2 earthquake affected Baja California, Mexico on April 4, 2010, and significant displacements were observed around the Laguna Salada Fault. The distribution of crustal movements is an effective source of information to estimate the fault-slip mechanism. In this study, one pre-event and one post-event radar images taken by the ALOS PALSAR sensor were used to detect geodetic deformation around the fault by a differential interferometric (DInSAR) analysis. Firstly, an initial DInSAR result was obtained from the pre- and post-event phase data. Then the fringe caused by coseismic deformation was obtained by removing the orbital fringe, topographic fringe and noises. Two unwrapping approaches were applied to transform the discontinuous fringe into actual displacements. The results were verified by comparing with a fault-slip model obtained from the global Centroid Moment Tensor (CMT) catalog. The phase unwrapping along the cross-section that was perpendicular to the fault showed a reasonable level of accuracy.

Keywords: Synthetic aperture radar (SAR) imagery, Differential interferometric analysis, Phase unwrapping, Fault-slip distribution

INTRODUCTION

A M_W 7.2 earthquake jolted Baja California, Mexico at 3:40 pm on April 4, 2010. The epicenter was located at 32.26° N, 115.29° W, with a shallow depth of 10 km. It occurred on the Laguna Salada Fault, which caused another M_W 7.2 earthquake in 1982. Due to the 120-km long rupture lasting for more than 45 seconds, many buildings and lifeline structures were damaged in the surrounding region. More than 200 people were injured and more than 25,000 people were affected by the earthquake. Due to the mainshock and continuous aftershocks, significant crustal displacements occurred around the fault. According to the data from GPS stations established by the California Real Time Network (CRTN) in the Unite Sates, more than 20 cm horizontal movements were observed after the mainshock. The GPS observation system is an effective tool to obtain precise movements. However, GPS stations have not been installed fully in all the parts of the world, especially in developing countries. In Mexico, only one station was installed in the middle of the country, far away from the Laguna Salada Fault. The displacements due to earthquakes can also be calculated from acceleration records observed by strong motion seismometers. Several researches have conducted the comparison between the coseismic displacements obtained from acceleration records and GPS observation data (Boore, 2001; Wu and Wu, 2007; Wang et al., 2013; Yamazaki et al., 2014). However, this method can obtain only the displacement occurred at the location of a seismometer. Thus, remote sensing technology using satellite images is an effective tool to grasp a large-scale coseismic deformation.

Interferometric analysis of synthetic aperture radar (SAR) is a useful method to detect spatially coherent ground information (Zebker, 2000). Many researchers have detected daily and coseismic displacements based on this method (Stramondo et al., 2002; Wicks et al., 2013). Interferometric analysis (InSAR) can detect displacements at the centimeter level, despite its meter-level image (pixel) resolution, but displacements can only be obtained in the line-of-sight direction. Another drawback of InSAR is that the method is applicable only for not-too-large coherent displacements. The cross-correlation (pixel-offset) method is an alternative for measuring the relative two-dimensional (2D)

[1] Assistant Professor, Chiba University, Chiba, Japan, wen.liu@chiba-u.jp
[2] Associate Professor, Tokyo Institute of Technology, Yokohama, Japan, matsuoka.m.ab@m.titech.ac.jp
[3] Professor, Chiba University, Chiba, Japan, fumio.yamazaki@faculty.chiba-u.jp

displacement between two images in a pixel to sub-pixel scale, such as in detecting coseismic deformation (Michel et al., 1999; Tobita et al., 2006). The ground displacements caused the 2010 Baja California earthquake were estimated by Matsuoka and Kodama (2011) from the pre- and post-event Terra ASTER and ALOS PRISM satellite optical images using the pixel-offset method. The wide-range displacements obtained from satellite images could provide useful information to estimate fault-slip distributions (Beavan et al., 2011; Jiang et al., 2013).

In this study, the displacements due to the earthquake around the Laguna Salada Fault are detected using the pre- and post-event ALOS PALSAR data by the differential InSAR analysis. The obtained phase is unwrapped by two methods and transformed into the actual movements observed in the sensor range direction. In addition, a fault model is built according to the parameters obtained from the Global Centroid-Moment-Tensor (CMT) Catalog (2010). The displacements simulated from the fault model are compared with our result in order to verify its accuracy.

STUDY AREA AND IMAGERY DATA

The study area focuses on the Laguna Salada Fault, located at the border of Mexico and the United States, shown in Fig. 1(a). According to the optical image shown in Fig. 1(b) from *Google Earth*, Mexicali city is located in the northeast (50 km) of the epicenter. Agricultural lands spread surrounding Mexicali, in the east and south parts of the fault. After the earthquake, widespread liquefaction was reported in the Mexicali Valley near the epicenter and caused significant damages (Earthquake Engineering Research Institute, 2010). There are three GPS stations established by CRTN. From all the three stations, southeastward displacements were observed after the mainshock. The maximum of horizontal movement was observed at the station "P496", which was 19.1 cm to the south and 4.9 cm to the east. Since all the three stations were estimated in the north of the fault, it is difficult to grasp the overall movements cause by the earthquake only from the GPS observation data.

The pre- and post-event PALSAR data were used to detect the deformation in the target area. PALSAR is an active microwave sensor loaded on the Advanced Land Observing Satellite (ALOS) launched in 2006, using L-band frequency with 23.6 cm wavelength. Different from optical sensors, SAR data can be acquired at both daytime and nighttime despite of weather conditions. Thus, it is more suitable for mapping damaged areas reliably and promptly after the occurrence of disasters. It had stopped working after the 2011 Tohoku, Japan earthquake in May 2011. However, a follow-on satellite (ALOS-2) with the new PALSAR-2 sensor has been launched in May 24, 2014, providing higher resolution images. The pre-event PALSAR data used in this study was taken on December 16 (local time), 2009 whereas the post-event one on May 3, 2010, almost one month after the mainshock. The incident angle was 38.6° at the center of the images, with a heading of 350.4° clockwise from the north. The pre-event data was captured with horizontal/horizontal (HH) polarization in the Fine Beam Single (FBS) mode. The resolution was 3.1 m in the azimuth direction and 4.7 m in the range direction. The post-event data was captured with HH and horizontal/vertical (HV) polarizations in the Fine Beam Dual (FBD) mode, with 3.1 m resolution in the azimuth- and 9.4 m in the range-direction.

Two data were provided as the received signal data with the processing level 1.0. Several pre-processing steps were carried out using *ENVI/SARscape* software. After the range and azimuth compressing, the data were transformed to the Single-Look Complex (SLC) products including both the intensity and phase information. A multi-looking process was applied to the azimuth direction, and then the resolution in the azimuth directions was changed to 12.4 m. A 90 m Shuttle Radar Topography Mission (SRTM) digital elevation model (DEM), as shown in Fig. 2(a), was introduced to project the data to a WGS84 reference ellipsoid with a resampled square pixel size of 15 m. A color composite image of the pre- and post-event intensity images was generated and shown in Fig. 2(b). Significant changes in the backscattering intensity could be confirmed in agricultural lands. However, it is difficult to identify these changes whether temporal agriculture changes or damages. Seasonal differences in the water level caused the backscatter changes in the western part of the fault. Surface rupture could not be observed from the SAR intensity images.

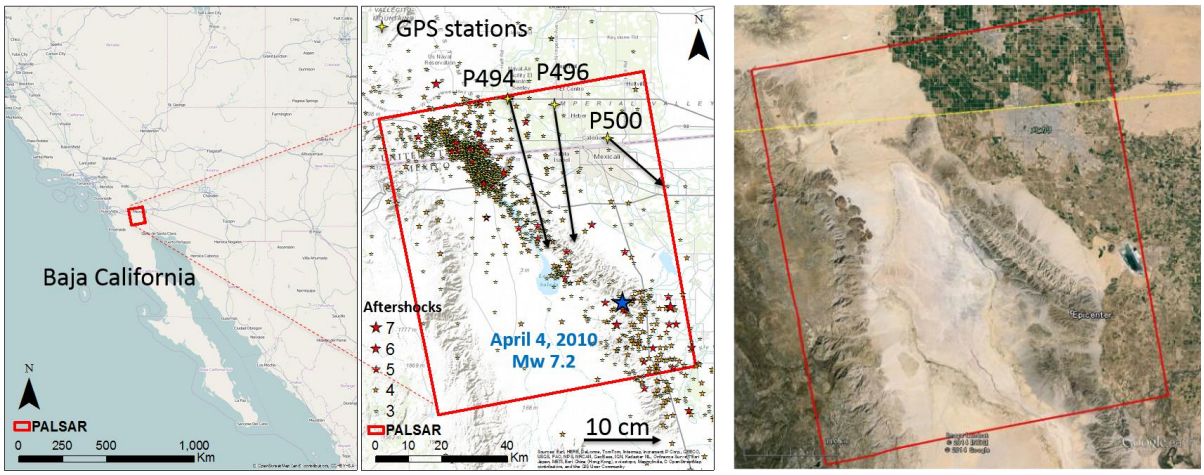

(a) Study area (b) Optical image from Google Earth

Figure 1. Study area around the Laguna Salada Fault in Baja California, Mexico, including three GPS stations established in the United States (a); the blue star mark is the epicenter of the mainshock whereas the others are those of the aftershocks larger than M_w 3 until May 4, 2010; an optical satellite image of the target area taken on April 10, 2013 from *Google Earth* (b).

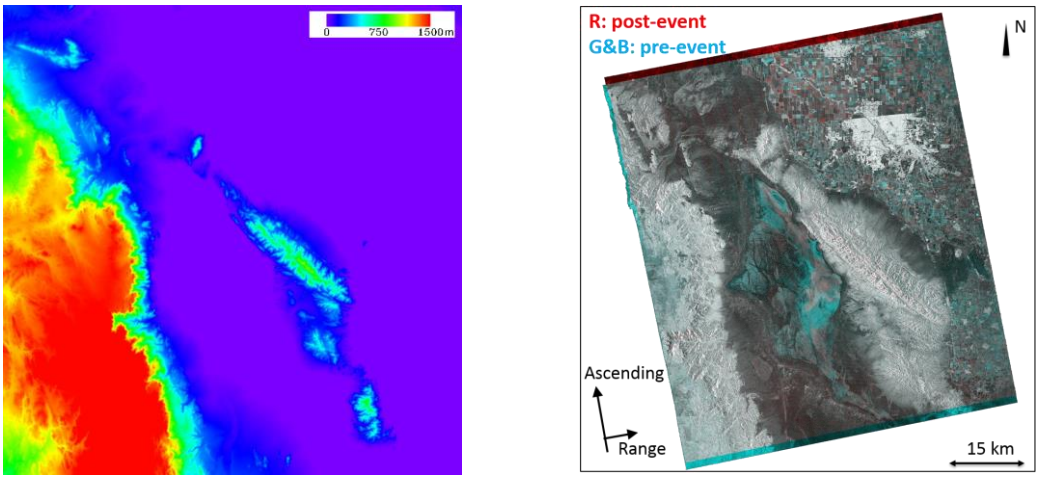

(a) Digital elevation model (DEM) (b) Color composite SAR images

Figure 2. 90 m resolution SRTM digital elevation model used in this study (a); a color composite of the pre- and post-event PALSAR intensity images, geocoded into UTM projection (b).

DISPLACEMENT DETECTION BY INTERFEROMETRIC SAR ANALYSIS

InSAR analysis is a radar techniques used to generate maps of surface deformation or digital elevation, using the phase differences of the waves between two or more SAR data. An InSAR analysis was applied to the two SLC products of PALSAR using *ENVI/SARscape* software. The flowchart of approaches is shown in Fig. 3(a). First, an initial InSAR result was obtained using the two complex imagery data. The SRTM DEM was introduced to remove elevation and orbital effects from the initial result. And, noises were removed by the Goldstein filter (Goldstein and Werner, 1998). Then the final interferogram including only the fringe caused by coseismic deformation was obtained. In addition, a coherence map, which represents the quality of interferogram, was calculated with the value between 0 and 1. Finally, the final interferogram and coherence images were projected into a geo-referenced map.

Although the temporal difference between the pre- and post-event data is 138 days and the spatial baseline distance is 988 m, most of the target areas show high coherence. The final inteferogram is shown in Fig. 3(b) and the coherence map is shown in Fig. 3(c). The fringe caused by the coseismic deformation between $-\pi$ and π was obtained from the areas with higher coherence than 0.25. One

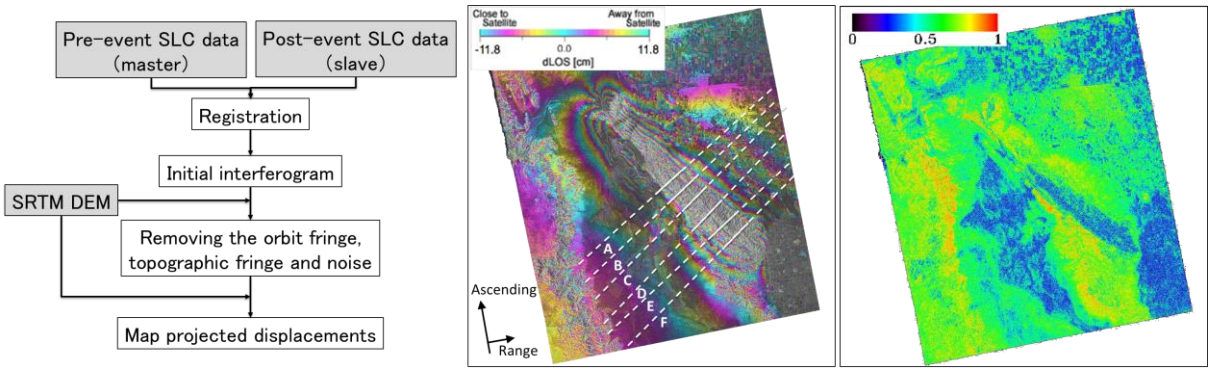

(a) Flowchart of process (b) Deformation fringe (c) Coherence

Figure 3. Flowchart of the process in the DInSAR analysis (a); the fringe caused by coseismic deformation obtained by removing orbit fringe, topographic fringe and noises from the initial interferogram (b), and the coherence calculated from the phase information (c)

cycle represents 11.8 cm displacement which is half of the wavelength. The low coherence shown in the middle of the fault with no change in the backscattering intensity, is considered to be caused by significant local movements. The interforegram at the border of the western mountain area shows noises even with the higher coherence than 0.7. These errors caused by severe changes in elevation.

An unwrapping step is essential to connect discontinuous fringes into a continuous displacement. Two different methods were used in this study. First, the fringes in the whole target area with the higher coherence than 0.25 were unwrapped by the Minimum Cost Flow method (Costantini, 1998). This method considers a square grid over the image pixels, and is enable to overcome the presence of large areas with low coherence. To remove the phase offset, ground control points (GCPs) were required after unwrapping. Normally, the locations and observed records of GPS stations are used as GCPs. However, the GPS stations within the target area are all in the north and difficult to refine the phase. Then seven points were selected manually in the stable area with high coherence and far away from the fault, as shown in Fig. 4(a). Since the displacements by the GPS are unavailable, they were considered as fixed points. The displacements in the line-of-sight direction were obtained and shown in Fig. 4(a).

The movements in different directions were observed from the obtained result. The west side of the Laguna Salada Fault moved close to the sensor direction, which represents the horizontal movement to the southwest or vertical uplift. In contract, the eastern side moved away which represents a northeastward horizontal movement or a subsidence occurred. The maximum of 1.5 m far-away and 0.5 close-ward displacements were detected. The displacements in six sections perpendicular to the fault are recorded in Fig. 5 as "PALSAR_1". The sections are about 6 km long and shown in Fig. 4(a) by red lines. In the section A to C, almost no displacement was detected in the west-side of the fault, whereas more than 0.3 m far-away movements were observed in the east-side. In the section D to F, about 0.2 m close-ward and 0.2 m far-way movements were detected in the west and east side, respectively. The average of the detected displacement in the east- and west-side of the fault were calculated and summarized in Table 1. Generally, the displacements detected by the Minimum Cost Flow method are smaller to those reported in the field survey (Earthquake Engineering Research Institute, 2010). In addition, the boundary of the fault plane is difficult to identify from the result due to the smoothing grid.

The second unwrapping method is connecting phases directly in the direction perpendicular to the fault. Six sections were extended as the dotted lines in Fig. 3(b). The distances between the center of the fault and the ends of section are approximately 30 km. The unwrapping process was carried out from the end to the center, in the east-side and west-side, respectively. The ends in the both sides were considered as the fixed points without displacement. Then the difference in the phase between two neighboring pixels along the section was calculated. Since the fringe is in between $-\pi$ and π, the phase is considered as a new repeat cycle if the difference is larger than $\pm$ 4.5 rad. 2π ambiguity was

calibrated for each repeat cycle. Finally, the unwrapped phase was transformed into displacements in the sensor range direction. The obtained displacements in the same six sections are plotted in Fig. 5 as "PALSAR_2".

Lager displacements were detected by the second unwrapping method. Same trend of movements were observed from the result. In the sections A to D, the west side of the fault moved 0.5 m close to the sensor direction, whereas the sections E and F moved 0.3 m. In the east side, more than 0.5 m far-away movements were detected in five sections except for the section E. Since the unwarping began from the two sides and ended in the middle, the boundary of the fault plane is clear. The average of the detected displacements in the east- and west-side of the fault was calculated and listed in Table 1.

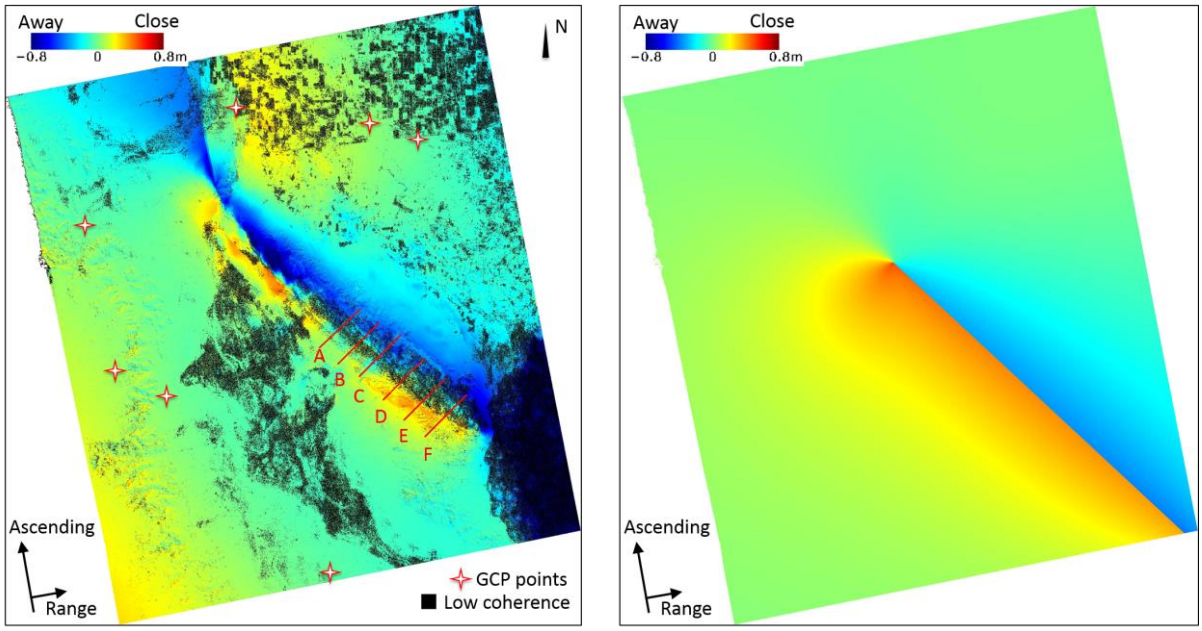

(a) Displacement obtained by DInSAR analysis (b) Simulated displacements

Figure 4. Displacements in the range direction, detected by unwrapping the fringes obtained from DInSAR analysis as a whole (a) and simulated from a CMT fault model (b)

VERIFICATION AND DISCUSSION

A fault mode was built to verify the obtained results from the PALSAR data. The parameters published in the Global Centroid Moment Tensor (CMT) catalog (2010) for the mainshock were adopted. From the observation data of six strong motion seismometers, a CMT solution was calculated with the centroid location at 32.31° N, 115.39° W and 12.8 km depth. Two planes were obtained with 223° and 313° strike angles. The plane with 313° strike, 88° dip and -174° rake was used according to the InSAR result and the aftershocks show in Fig. 1(a). The length of fault plane is about 66 km and the width is 20 km. Since the location of the fault plane did not match with the results from PALSAR precisely, it was shifted to the southwest to match with the center of the fault. Then three-dimensional (3D) displacements in the east, north and vertical directions were simulated by a rectangular dislocation in homogeneous and elastic half-space (Okada, 1985).

According the slip distribution, the east-side of the fault moved to the southeast. The maximum of predicted displacements was 0.55 m to the east and 0.82 m to the south. The west-side of the fault moved to the northwest, with the maximum of 0.87 m westward displacement and 0.49 m northward displacements. In the vertical direction, the east side subsided about 8 cm whereas the west side uplifted 7 cm. Since the displacements detected from the PALSAR data were observed in the line-of-sight direction, the simulated 3D movements need to be transformed into the slant-range direction. The relationship between an actual movement (*D*) to the east-, north- and vertical-directions, and its shift (*Ms*) captured to the line-of-sight direction is represented by Eq. (1).

$$M_s = \left(-D_E \sin\alpha + D_N \cos\alpha\right)\sin\theta + D_Z \cos\theta \tag{1}$$

where α is the heading angle clockwise from the north, and θ is the SAR incident angle.

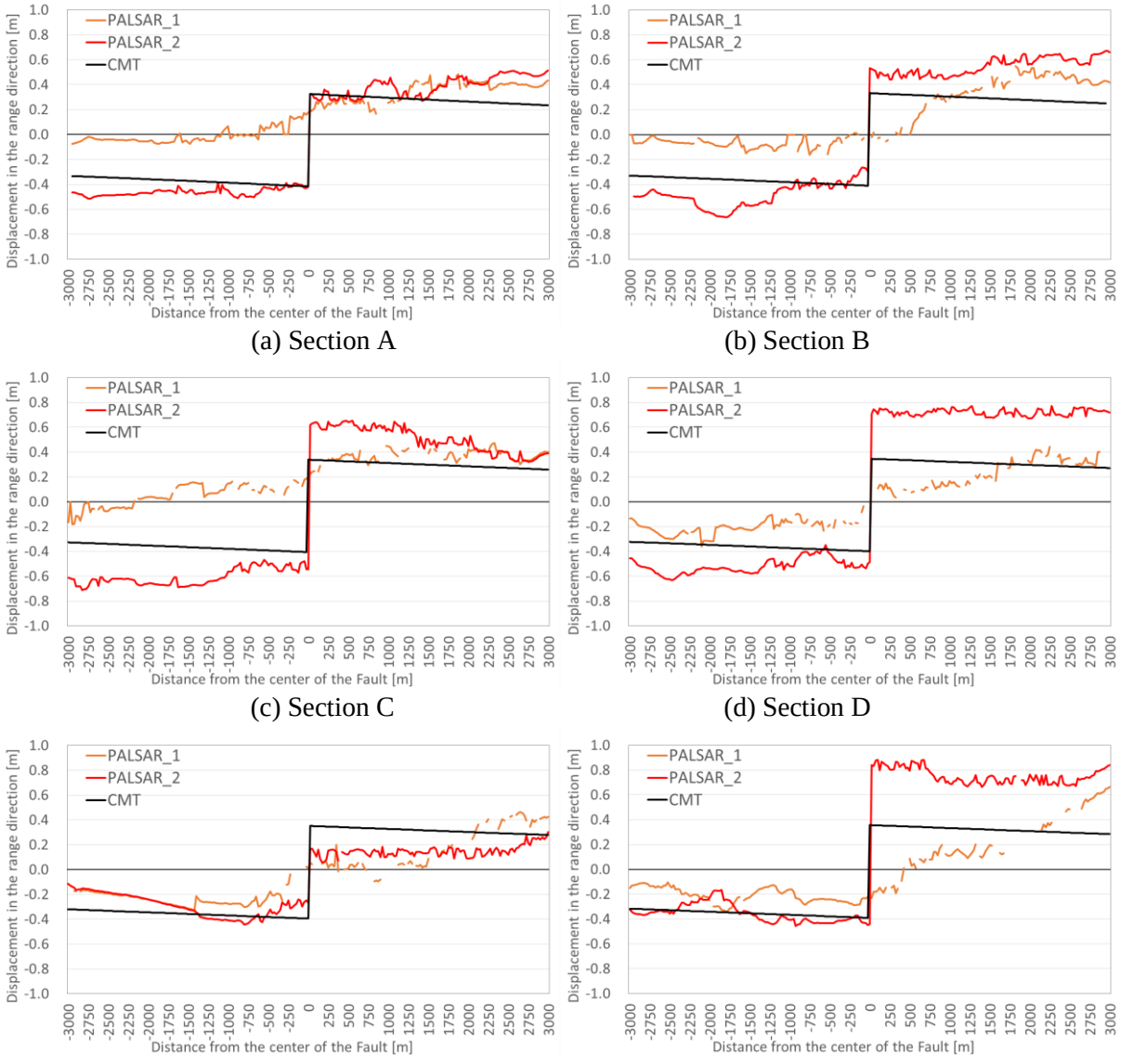

(a) Section A (b) Section B

(c) Section C (d) Section D

(e) Section E (f) Section F

Figure 5. Displacements in six sections of Figure 4(a), detected by unwrapping the fringes obtained from the InSAR analysis generally (PALSAR_1), unwrapping along the section direction (PALSAR_2) and simulated from the CMT fault model (CMT).

Table 1. Average value of displacements in the East- and West-side of the fault obtained from the PALSAR images and simulated from the CMT fault model.

	A		B		C		D		E		F	
	West	East	West	East	West	East	West	East	West	East	West	East
PALSAR_1	-0.01	0.35	-0.07	0.35	0.05	0.37	-0.20	0.23	-0.23	0.16	-0.21	0.20
PALSAR_2	-0.46	0.39	-0.48	0.55	-0.61	0.50	-0.52	0.72	-0.29	0.15	-0.36	0.75
CMT	-0.37	0.28	-0.37	0.29	-0.37	0.29	-0.36	0.30	-0.36	0.30	-0.35	0.31

Due to the observing mode, the heading angle and the incident angle were different in each pixel. Thus, the simulated displacement in the line-of-sight direction was calculated for each pixel, and is shown in Fig. 4(b). Same trend of movements were obtained from the fault model. Largest displacements occurred close to the bounder of the fault plane, and became smaller as going away. Comparing with the displacements in Fig. 4(a), the fault plane obtained from the simulation was shorter than that obtained from the PALSAR data. According to the report (Southern California Seismic Network, 2010), the fault plane extended to the border with the Unite States and the surface rupture became larger after April 5, 2010 due to frequent aftershocks. Since the post-event data was taken on May 3, the displacements detected from PALSAR includes the influence of the aftershocks.

The simulated displacements in the six sections are also plotted in Fig. 5 as "CMT" whereas the average values in the east and west sides are shown in Table 1. Generally, the displacements obtained by the second unwrapping method showed better agreement than those by the first method. In sections A and E, the "PALSAR_2" displacements almost matched with the simulated ones from the fault model. In other sections, the "PALSAR_2" showed the same trend but larger values than those from the simulation. As already has mentioned, the surface rupture became larger due to the afterschoks. Thus, larger movements could be observed from PALSAR data in theory. The results obtained by the second method exhibited good accuracy, and the method can be used to estimate a precise fault-slip distribution.

CONCLUSIONS

The displacements due to the 2010 Baja California earthquake were detected from the pre- and post-event ALOS PALSAR satellite images. The phase differences caused by the coseismic deformation were obtained after removing the orbitial fringe, topographic fringe and noise using the interferometric SAR analysis. Two unwrapping methods were applied to connect repeat cycle phases into a continuous one, which corresponds to the displacement in the line-of-sight direction. The first method could obtain the displacements for the whole target area, however, the results were smoothened. The second method was applied to six sections that are perpendicular to the fault and larger displacements were obtained.

To verify our results, a fault model according to the Globule CMT solution was built. The results obtained from the PALSAR data were compared with the simulated displacements from the fault model. It was confirmed that the detection using PALSAR data could grasp the overall trend of deformation. Since the fault model was calculated from the seismic waves from the mainshock, the simulated displacements were smaller than the actual ones. Thus, the movements obtained by the second unwrapping method, which is a little larger than the simulation, are considered as good results.

In the future, the displacements in the whole area will be calculated by the second unwrapping method. Additional information on the actual movements will be used to calibrate the reference points. Finally, a new fault-slip distribution including the aftershocks will be estimated using the displacements obtained from the PALSAR data.

ACKNOWLEDGMENTS

The ALOS PALSAR data used in this study owned by Japanese Space Agency (JAXA) and Japanese Ministry of Economy, Trade and Industry (METI).

REFERENCES

Beavan, J., E. Fielding, M. Motagh, S. Samasonov and N. Donnelly (2011). "Fault location and slip distribution of the 22 February 2011 Mw 6.2 Christchurch, New Zealand, earthquake from geodetic data", *Seismological Research Letters*, **82** (6), pp. 789-799.

Boore, D. (2001). "Effect of Baseline Corrections on Displacements and Response Spectra for Several Recordings of the 1999 Chi-Chi, Taiwan, Earthquake", *Bulleting of the Seismological Society of America*, **91**, 1199-1211.

Costantini, M. (1998). "A novel phase unwrapping method based on network programming", *IEEE Transactions on Geoscience and Remote Sensing*, **36**(3), 813-821.

Earthquake Engineering Research Institute (2010). "Learning from earthquakes: The Mw 7.2 EL Mayor Cucapah (Baja California) earthquake of April 4, 2010", EERI Special Earthquake Report, 1-12.

Goldstein, R.M. and C.L. Werner (1998). "Radar Interferogram Filtering for Geophysical Applications", *Geophysical Research Letter*, **25**(21), 4035-4038.

Global Centroid-Moment-Tensor (CMT) Project (2010): http://www.globalcmt.org/

Jiang, G., C. Xu, Y. Wen, Y. Liu, Z. Yin and J. Wang (2013). "Inversion for coseismic slip distribution of the 2010 Mw 6.9 Yushu Earthquake from geodetic data", *Geophysical Journal International*, 1-12.

Matsuoka, M. and S. Kodama (2011). "Coseismic displacement measurement of the 2011 EL Mayor, Mexico Earquake by subpixel correlation from optical satellite images", *IEEE International Geoscience and Remote Sensing Symposium (IGARSS)*, 4010-4013.

Michel, R., J.-P. Avouac and J. Taboury (1999). "Measuring ground displacements from SAR amplitude image: Application to the Landers earthquake", *Geophysical Research Letters*, **26**(27), 875-878.

Okada, Y. (1985). "Surface deformation due to shear and tensile faults in a half-space", Bulletin of the Seismological Society of America, **75**, 1135–1154.

Southern California Seismic Network (2010): http://www.scsn.org/2010sierraelmayor.html

Stramondo, S., F.R. Cinti, M. Dragoni, S. Salvi and S. Santini (2002). "The August 17, 1999 Izmit, Turkey, earthquake: Slip distribution from dislocation modeling of DInSAR and surface offset", *Annals of Geophysics*, **45**(3/4), 527-536.

Tobita, M., H. Suito, T. Imakiire, M. Kato, S. Fujiwara and M. Murakami (2006). "Outline of vertical displacement of the 2004 and 2005 Sumatra earthquakes revealed by satellite radar imagery", *Earth, Planets and Space*, **58**(1), e1-e4.

Wicks, C., C. Weaver, P. Bodin and B. Sherrod (2013). "InSAR evidence for an active shallow trust fault beneath the city of Spokane Washington, USA", *Journal of Geophysical Research: Solid Earth*, **118**, 1-9.

Wang, R., S. Parolai, M. Ge, M. Jin, T.R. Walter and J. Zschau (2013). "The 2011 Mw 9.0 Tohoku Earthquake: Comparison of GPS and Strong-Motion Data", *Bulletin of the Seismological Society of America*, **103**, 1336–1347.

Wu, Y. and C. Wu (2007). "Approximate recovery of coseismic deformation from Taiwan strong-motion records", *Journal of Seismology*, **11**, 159-170.

Yamazaki, F., L. Moya, K. Anekoji and W. Liu (2014). "Comparison of coseismic displacements obtained from strong motion accelerograms and GPS data in Japan", *Proceedings of the Second European Conference on Earthquake Engineering and Seismology*, Istanbul, Turkey, 10p.

Zebker, H.A. (2000) "Studying the Earth with interferometric radar", *IEEE Computing in Science & Engineering*, **2**(3), 52-60.